Evaluation of tumor localization in respiration motion-corrected cone-beam CT: Prospective study in lung

Oleksandr Dzyubak, Russell Kincaid, Agung Hertanto, Yu-Chi Hu, and Hai Pham
Department of Medical Physics, Memorial Sloan-Kettering Cancer Center, New York, New York 10065

Andreas Rimner
Department of Radiation Oncology, Memorial Sloan-Kettering Cancer Center, New York, New York 10065

Ellen Yorke, Qinghui Zhang, and Gig S. Mageras[a)]
Department of Medical Physics, Memorial Sloan-Kettering Cancer Center, New York, New York 10065

(Received 24 April 2014; revised 5 September 2014; accepted for publication 5 September 2014; published 1 October 2014)

Purpose: Target localization accuracy of cone-beam CT (CBCT) images used in radiation treatment of respiratory disease sites is affected by motion artifacts (blurring and streaking). The authors have previously reported on a method of respiratory motion correction in thoracic CBCT at end expiration (EE). The previous retrospective study was limited to examination of reducing motion artifacts in a small number of patient cases. They report here on a prospective study in a larger group of lung cancer patients to evaluate respiratory motion-corrected (RMC)-CBCT ability to improve lung tumor localization accuracy and reduce motion artifacts in Linac-mounted CBCT images. A second study goal examines whether the motion correction derived from a respiration-correlated CT (RCCT) at simulation yields similar tumor localization accuracy at treatment.

Methods: In an IRB-approved study, 19 lung cancer patients (22 tumors) received a RCCT at simulation, and on one treatment day received a RCCT, a respiratory-gated CBCT at end expiration, and a 1-min CBCT. A respiration monitor of abdominal displacement was used during all scans. In addition to a CBCT reconstruction without motion correction, the motion correction method was applied to the same 1-min scan. Projection images were sorted into ten bins based on abdominal displacement, and each bin was reconstructed to produce ten intermediate CBCT images. Each intermediate CBCT was deformed to the end expiration state using a motion model derived from RCCT. The deformed intermediate CBCT images were then added to produce a final RMC-CBCT. In order to evaluate the second study goal, the CBCT was corrected in two ways, one using a model derived from the RCCT at simulation [RMC-CBCT(sim)], the other from the RCCT at treatment [RMC-CBCT(tx)]. Image evaluation compared uncorrected CBCT, RMC-CBCT(sim), and RMC-CBCT(tx). The gated CBCT at end expiration served as the criterion standard for comparison. Using automatic rigid image registration, each CBCT was registered twice to the gated CBCT, first aligned to spine, second to tumor in lung. Localization discrepancy was defined as the difference between tumor and spine registration. Agreement in tumor localization with the gated CBCT was further evaluated by calculating a normalized cross correlation (NCC) of pixel intensities within a volume-of-interest enclosing the tumor in lung.

Results: Tumor localization discrepancy was reduced with RMC-CBCT(tx) in 17 out of 22 cases relative to no correction. If one considers cases in which tumor motion is 5 mm or more in the RCCT, tumor localization discrepancy is reduced with RMC-CBCT(tx) in 14 out of 17 cases ($p = 0.04$), and with RMC-CBCT(sim) in 13 out of 17 cases ($p = 0.05$). Differences in localization discrepancy between correction models [RMC-CBCT(sim) vs RMC-CBCT(tx)] were less than 2 mm. In 21 out of 22 cases, improvement in NCC was higher with RMC-CBCT(tx) relative to no correction ($p < 0.0001$). Differences in NCC between RMC-CBCT(sim) and RMC-CBCT(tx) were small.

Conclusions: Motion-corrected CBCT improves lung tumor localization accuracy and reduces motion artifacts in nearly all cases. Motion correction at end expiration using RCCT acquired at simulation yields similar results to that using a RCCT on the treatment day (2–3 weeks after simulation). [http://dx.doi.org/10.1118/1.4896101]

Key words: cone-beam computed tomography, image-guided radiation treatment, organ motion, lung cancer

1. INTRODUCTION

Tumor motion, caused by respiration, introduces a source of geometrical uncertainty in radiation therapy, which requires appropriate management to avoid marginal misses and target underdosage.[1–3] Since respiratory motion is known to be patient-specific and variable from cycle to cycle, respiration-correlated cone-beam CT (RC-CBCT) has been investigated

for radiation treatment in lung.[4–6] The main advantage of RC-CBCT is that localization with reduced blurring and motion extent determination can be examined immediately before radiotherapy. Clinical usage of RC-CBCT has been reported for localization in lung[3,4,7–13] and liver.[14] Disadvantages of using respiration-correlated CBCT are long scan times and view aliasing artifacts caused by sparse projections.[4–6]

Various techniques have been investigated to correct motion artifacts in the CBCT. Brehm *et al.*[15] used a cyclic registration that effectively suppresses streak artifacts in images acquired with a standard protocol without adaptive or slow gantry rotation. Such a technique is resistant to sparse view artifacts and can reconstruct temporal images of high quality even in cases with short patient breathing cycles relative to the acquisition time. In the approach by Li and Xing,[16] the CBCT image data acquisition protocol was modified by changing gantry rotation speed optimized in accordance with patient-specific breathing tumor motion. Lauzier *et al.*[17] have investigated an approach for reconstructing respiration-correlated CBCT sparse projections based on prior image constrained compressed sensing. Rit *et al.* reported on a method to correct for respiratory motion during reconstruction of CBCT images using an *a priori* motion model of the patient respiratory cycle estimated from the respiration-correlated CT (RCCT) planning CT.[18]

These studies were retrospective and focused on CBCT image quality. In the reconstructed images, tumor and organ localization accuracy could not be evaluated due to a lack of a criterion standard.

Previously we have reported on a method to correct respiratory motion artifacts in 1-min CBCT scans, using a patient-specific motion model derived from a respiration-correlated image set.[19] In a retrospective study of patient images, the method was shown to be applicable in both thorax and abdomen. The previous study examined a limited number of patient cases and tumor localization accuracy could not be measured due to a lack of a criterion standard for comparison. In the method's application to thorax, the prior study used the same CBCT images for both deriving the patient-specific motion model and for motion correction. The rationale for this approach was that it required no assumptions of sameness of anatomical deformations between model-derivation and motion-corrected imaging sessions. A limitation of this approach, however, was that the respiration-correlated data derived from the CBCT contained strong view aliasing artifacts which adversely affected the deformable image registration used to obtain the motion model.

We report here on a prospective clinical study of motion-corrected CBCT in lung cancer patients. We examine the method's efficacy in improving localization accuracy as well as reducing motion artifacts in 1-min CBCT scans. In this study, higher quality RCCT scans are used to derive the patient-specific motion model, as an alternative to using CBCT images. Since the clinical process commonly acquires RCCT at simulation, a consideration is whether the patient tumor-motion pattern may change between simulation and treatment. Therefore, a further study goal is to examine whether the motion correction derived from RCCT at simulation yields similar tumor localization accuracy at treatment.

2. MATERIALS AND METHODS

2.A. Patient characteristics and image acquisition

In an IRB-approved prospective study with informed consent, data from 19 lung cancer patients (22 tumors) were collected and analyzed. Tumors were in various locations of both lungs and had gross tumor volumes (GTVs) ranging from 1 to 311 cm^3. Two patients exhibited multiple tumors.

The images to be used in this study were acquired at both the simulation and treatment day. On simulation day, patients received a free-breathing helical CT scan (8-slice LightSpeed, GE Healthcare, Waukesha, WI) for treatment planning purposes (referred to here as plan CT). This was followed by a respiration-correlated CT [referred to here as RCCT(sim)] acquired in axial cine mode with respiratory signal recorded by the RPM system (Real-time Position Management, Varian Medical Systems, Palo Alto, CA). Cine acquisition time per couch position was set to the patient's respiration period (measured with RPM) plus 1 s, with gantry rotation period of 0.5 s. The time interval between consecutive images was the greater of either 1/20 of the respiration period or 0.25 s, thus yielding 20 or more repeat images at each couch position. Reconstructed CT slice thickness was 2.5 mm. Since commonly used phase-based sorting of RCCT often results in discontinuity artifacts caused by amplitude variations in breathing, an amplitude-based sorting approach was used instead,[20,21] to produce a ten-bin RCCT image set. The use of amplitude binning is not a requirement. However, Hertanto *et al.*[20] showed that the amplitude binning approach reduced artifacts in RCCT images caused by irregular breathing. Thus for our study, we have used the amplitude binning approach. Briefly, images were binned according to RPM amplitude, yielding five bins (0th-to-10th, 10th-to-20th, etc., through 40th-to-50th percentiles) along the expiration portion of the breathing cycle, and five bins (50th-to-60th through 90th-to-100th percentiles) along inspiration. In cases where amplitude-based sorting resulted in missing image data or gaps in the CT slices, the RCCT set was generated using a motion model predictive procedure described by Hertanto *et al.*[20]

On one treatment day in the first week of treatment, patients received the following scans: a respiration-correlated CT just before or after the treatment session [referred to as RCCT(tx)], a respiration-gated CBCT, and a clinical nongated CBCT. RCCT(tx) acquisition was similar to that for RCCT(sim). The CBCT scans were acquired on a TrueBeam Linac (version 1.5, Varian Medical Systems). The gated CBCT was carried out in TrueBeam Developer Mode and consisted of gated gantry rotation and kilovolt projection image acquisition using a programmable script.[11] The Developer Mode was only used for imaging patients and not for treatment. As such IRB determined that investigational device exemption was not needed for this study. The gate was centered at end expiration (EE) with approximately 35% duty cycle (range 25%–50%), resulting in a scan time of approximately 4 min (range 3–6 min). The resultant CBCT images exhibited reduced artifacts and served as a criterion standard for evaluating tumor localization accuracy and in the clinical CBCT images before and after respiratory motion correction (described further below).

TABLE I. Tumor characteristics.

Tumor number	Volume (cm^3)	Location in lung	Motion amplitude at simulation (cm)	Motion amplitude at treatment (cm)
1	7.8	Right	0.8	1.4
2	3.4	Right	0.9	1.3
3	1.7	Right	0.7	1.0
4	2.3	Left	0.6	2.3
5	9.3	Left	1.7	2.0
6	40.2	Right	0.6	0.9
7	2.8	Right	1.5	1.3
8	4.4	Left	1.1	0.9
9	9.4	Right	0.6	0.6
10	4.3	Right	0.9	1.3
11	49.8	Right	0.5	0.8
12	6.3	Right	0.3	0.5
13	4.7	Left	0.7	0.6
14	311.5	Right	0.6	0.9
15	38.4	Left	0.3	0.3
16	2.6	Left	0.5	0.4
17	5.0	Left	0.6	0.6
18	83.9	Right	0.4	0.5
19	1.0	Left	0.1	0.3
20	48.9	Right	0.4	0.6
21	5.6	Right	0.9	1.2
22	73.4	Left	0.6	1.1

All gated CBCT scans were performed under supervision by a physicist. The nongated CBCT, of 1-min duration, and patient treatment were delivered using the Linac's clinical mode of operation. Imaging parameters for the gated CBCT were similar to those for the nongated CBCT, i.e., 125 kV(peak), 80 mA, 20 ms, 11 images/s, half-fan acquisition (i.e., detector laterally offset 16 cm to obtain a 46 cm reconstructed diameter), and 360° rotation. The data collected using Developer Mode were not used to influence decisions about patient treatment.

Some characteristics of the tumors are provided in Table I.

2.B. Motion correction method

We briefly describe the process of generating a respiratory motion-corrected (RMC)-CBCT, which has been previously described in more detail.[19] Motion-corrected CBCT is based on a patient-specific motion model derived from a RCCT image set, either RCCT(sim) or RCCT(tx), and consists of multiple steps as depicted in Fig. 1. To derive a motion model, one of the images in the RCCT set is chosen as a reference, and deformable image registration of the remaining nine RCCT images to the reference image is performed, using a fast free-form algorithm.[27] Using principal component analysis (PCA), eigenmodes of the deformation vector fields (DVFs) are related to the displacement of a surrogate in the RCCT images relative to its position in the reference image. In our study we used the image at EE-image as the reference and the apex position (it is the most superior diaphragm point in the image set) of the ipsilateral diaphragm dome as a surrogate. At end expiration, the diaphragm is most superior which corresponds to the 40th-to-50th percentile bin in our amplitude binned data sets.

Two motion models are generated, one from the RCCT (sim), the other from RCCT(tx). Next, the motion model is applied to the 1-min CBCT scan as shown in Fig. 2. The CBCT projection images are amplitude sorted into ten bins based on the abdominal displacement measured by the Varian RPM system followed by reconstruction to produce a set of ten binned CBCT images. The reference binned CBCT image is chosen having the same bin index as the reference RCCT, and the surrogate displacement in each binned CBCT is determined relative to the reference CBCT. The surrogate displacements are input to the motion model, which deforms each binned CBCT to the reference state (EE), and all ten resultant images are summed to form a RMC-CBCT. We note that the differences in apparent brightness between the binned CBCT images in Fig. 2 are a result of differences in the number and angular arrangement of the projections, due to the amplitude binning. Although this procedure can be used to produce RMC-CBCT at any motion state, in this study end expiration was chosen for comparison with the gated CBCT.

2.C. Motion correction evaluation

The study compared clinical CBCT images without motion correction (baseline images) with respiratory motion-corrected CBCT images (test images), both reconstructed from the same 1-min scan. Respiration gated CBCT images[11] acquired at end expiration served as the criterion standard (Fig. 1). To confirm the validity of using the gated CBCT as

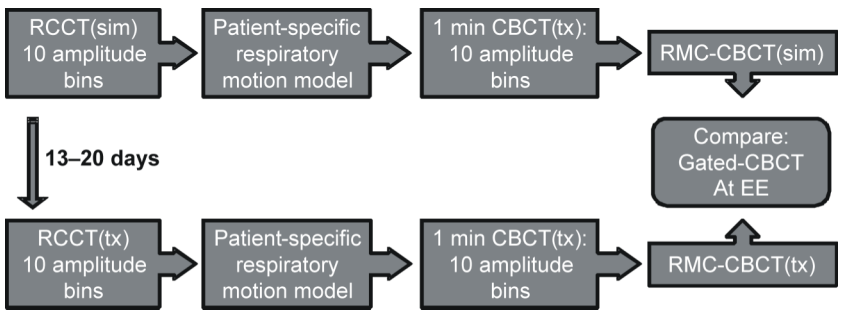

FIG. 1. Flowchart of the RMC-CBCT study design. RCCT(sim) denotes respiration-correlated CT at simulation; RCCT(tx) is acquired at treatment 13–20 days later. RMC-CBCT(sim) denotes correction derived from RCCT(sim); RMC-CBCT(tx) is derived from RCCT(tx). Gated CBCT is acquired at EE.

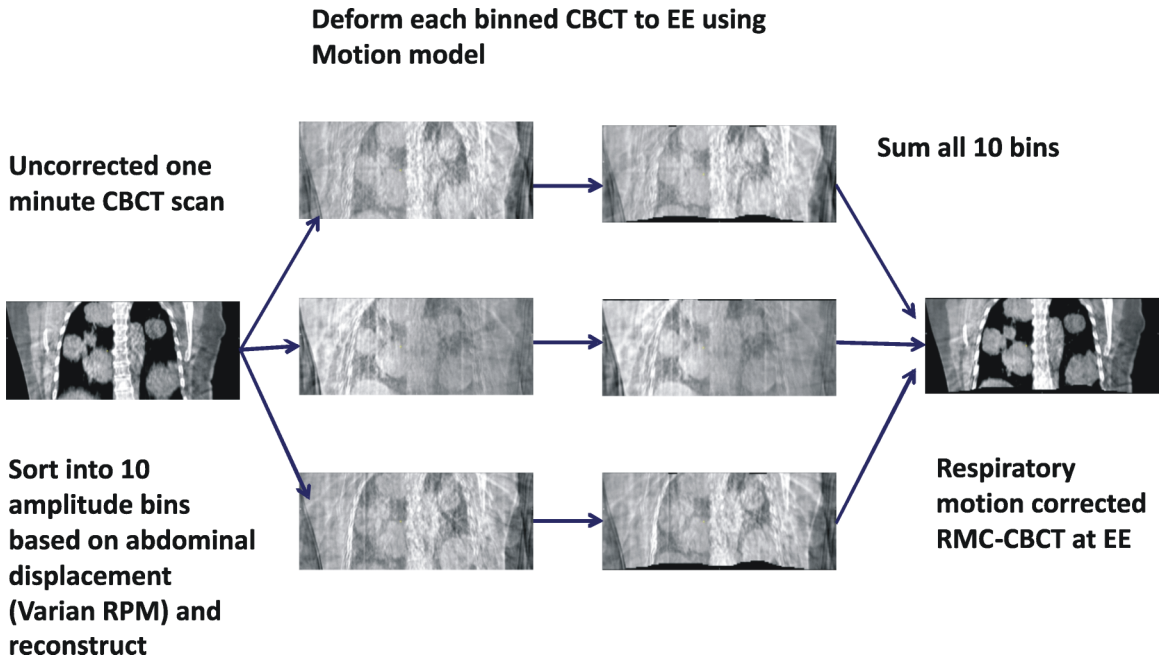

FIG. 2. Diagram illustrating formation of RMC-CBCT images. Same window/level display setting is used for the binned CBCT images (second and third columns); differences in brightness between binned CBCT images are a result of the amplitude sorting, see text. Same window/level display setting is used for the uncorrected CBCT and RMC-CBCT (first and fourth columns).

the ground truth for tumor location in the 1-min scan, first the binned CBCT images from the 1-min scan were selected whose RPM phase at the bin center was within the phase gate interval (typically 30%–65% RPM phase) in the gated scan. The selected binned CBCT images without correction for motion were summed and the tumor location in the resultant image was compared with that in the gated CBCT. The mean ± standard deviation discrepancy in tumor location was found to be 1.2 ± 0.6 mm.

Two motion-corrected images were produced for each patient: a RMC-CBCT(sim) image derived from the RCCT(sim) at simulation, and a RMC-CBCT(tx) image derived from the RCCT(tx) at treatment. The two types of motion-corrected images were compared to each other and to the CBCT without

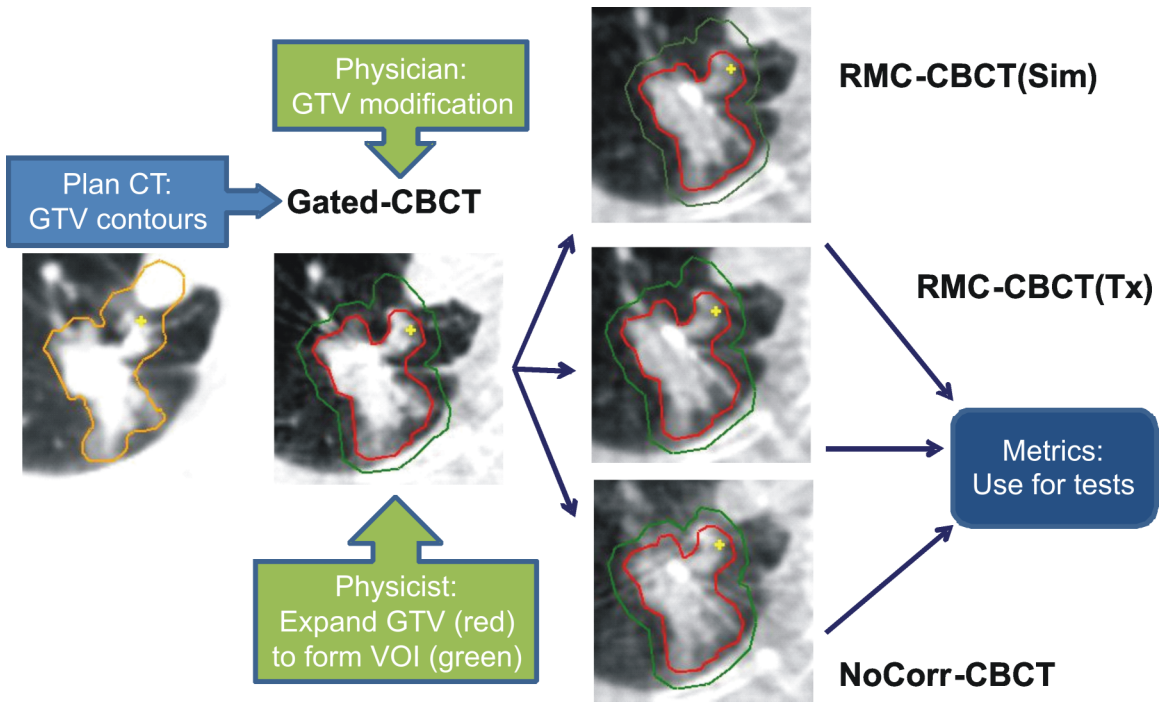

FIG. 3. Generation of GTV and VOI contours on CBCT image sets.

motion correction (NoCorr-CBCT). All reconstructions used the FDK algorithm that was part of a nonclinical research only software package (ITools-Reconstruction 1.0, Varian Medical Systems).[22]

Quantitative evaluation was based on tumor localization discrepancy and tumor NCC metrics. Localization discrepancy was measured by registering each image (baseline and test images) to the gated CBCT via alignment of the vertebral column, then measuring the difference in tumor centroid position between the two images. The latter was computed by rigid image registration (translations only) inside a volume-of-interest (VOI) containing the GTV so as to maximize a normalized cross correlation (NCC) of pixel intensities. Evaluation also compared the NCC coefficient within the VOI, between each of the test images and the gated CBCT. Following rigid image registration so as to align the tumor inside the VOI by maximizing NCC, the resultant NCC served as an additional metric of tumor localization accuracy for comparison. In order to quantify the reproducibility of the procedure, measurements were repeated five times: using two manually drawn rectangular box VOIs enclosing the GTV, each with two window-level display settings, and a fifth measurement using a VOI constructed by 3D expansion of the GTV by a 4 mm margin. For the first window-level within VOI, the average and standard deviation of intensities were calculated. Then window was chosen to be plus/minus two standard deviations about the average. Second settings shifted the window-level by 100 HU upward.

Delineation of the VOI was computed as shown in Fig. 3. First, the Plan-CT scan and GTV are exported from the treatment planning system (left panel in Fig. 3). The Plan-CT and gated CBCT images were rigidly registered by alignment of the vertebral column, and the GTV contours transferred from the Plan-CT to the gated CBCT. A radiation oncologist reviewed and modified (if needed) the transferred GTV contours (middle panel). Each test image [RMC-CBCT(sim), RMC-CBCT(tx), and NoCorr-CBCT] was aligned with the gated-CBCT by alignment of the vertebral column and the GTV and VOI contours transferred to the test image (right panel).

Evaluation also compared the NCC coefficient within the VOI, between each of the test images and the gated CBCT. Following rigid image registration so as to align the tumor inside the VOI by maximizing NCC, the resultant NCC served as an additional metric of tumor localization for comparison.

3. RESULTS

We first investigated whether the choice of diaphragm superior–inferior displacement was an appropriate surrogate for constructing the motion model by examining the correlation between diaphragm and tumor motion. Figure 4 shows, for both RCCT(sim) and RCCT(tx) data sets, the tumor centroid displacement between EE and end inspiration (EI) vs that for the diaphragm apex. For both data sets, the Pearson correlation coefficients were 0.60 and 0.72, respectively, thus confirming that tumor motion extent correlates with diaphragm motion extent.

Figure 5 qualitatively compares axial and sagittal views of one patient in the gated-CBCT, CBCT without motion correction (NoCorr), and RMC-CBCT(tx) images. As can be seen from the figure, blurring of the tumor and diaphragm (arrows) is reduced in RMC-CBCT compared to NoCorr-CBCT. Streak artifacts are reduced as well.

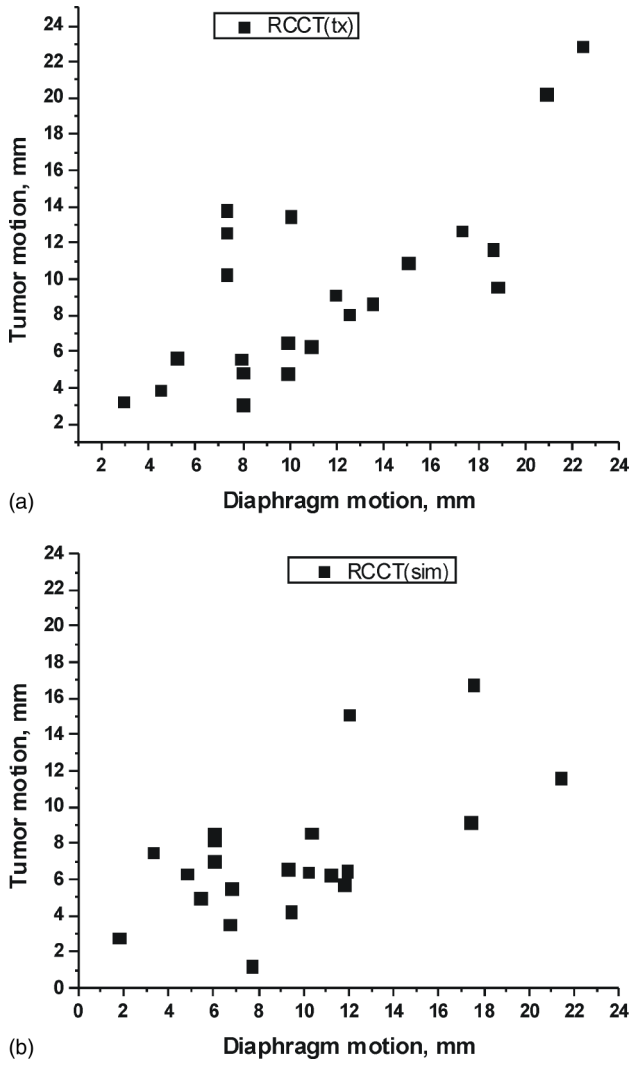

FIG. 4. Scatter plots of tumor EE-to-EI motion extent vs diaphragm EE-to-EI motion extent, for the RCCT image set (a) at simulation and (b) at treatment.

Figure 6(a) quantifies the tumor localization discrepancy, defined as the discrepancy in tumor position (3D distance), relative to the criterion standard (gated CBCT), of RMC-CBCT(sim), RMC-CBCT(tx), and NoCorr-CBCT.

Figure 6(b) shows differences in localization discrepancy between RMC-CBCT(tx) and NoCorr-CBCT, and between RMC-CBCT(tx) and RMC-CBCT(sim). In both plots, tumor cases are sorted in order of increasing difference in localization discrepancy [RMC-CBCT(tx) minus NoCorr-CBCT]. Figure 6(a) shows that 11 tumors have localization discrepancy greater than 2 mm without correction. We note that these values are larger than the discrepancy in tumor position (1.2 ± 0.6 mm) between gated and 1-min scans. In these 11 tumors, RMC-CBCT(tx) reduces localization discrepancy in all cases, whereas RMC-CBCT(sim) reduces the discrepancy in 9/11 cases. In 17 out of 22 cases, the tumor localization

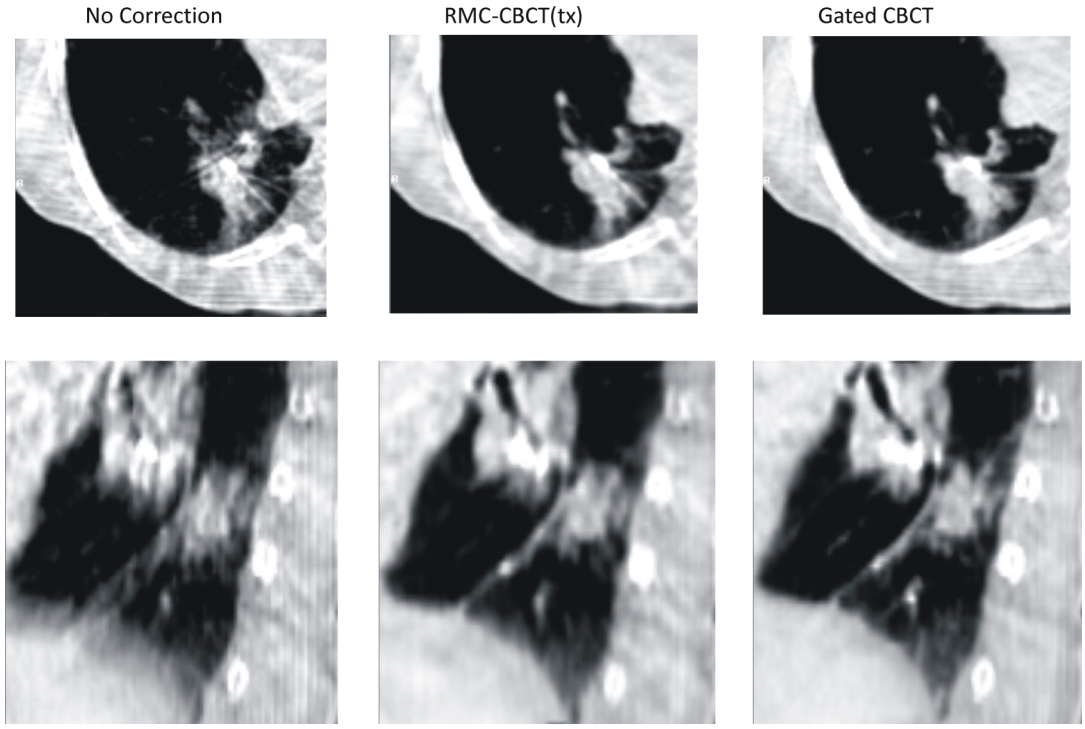

FIG. 5. Comparative example showing axial and sagittal images of a 1-min CBCT before motion correction (NoCorr CBCT), after motion correction [RMC-CBCT(tx)] derived from RCCT at treatment, and gated CBCT(gated-CBCT). Areas of tumor and diaphragm that are blurred in the NoCorr CBCT but show reduced blurring in the RMC-CBCT and gated CBCT. All images shown are mapped to a window-level of −250 HU and a window width of 900 HU.

discrepancy is lower in RMC-CBCT(tx) than in NoCorr-CBCT (light gray bars in both plots), but is not significant (two-sided paired t-test $p = 0.06$). In 13 out of 22 cases, the tumor localization discrepancy is lower in RMC-CBCT(tx) than in RMC-CBCT(sim) (white bars in both plots), but not significant ($p = 0.07$). If we limit the sample to cases in which tumor EE-to-EI excursion in the RCCT(tx) is 5 mm or more (cases labeled by an asterisk in Fig. 6), 14 out of 17 cases have lower localization discrepancy in the RMC-CBCT(tx) ($p = 0.04$). If we further consider cases in which tumor excursion is 5 mm or more in the RCCT at simulation, 13 out of 17 such cases show reduced localization discrepancy in RMC-CBCT(sim) images relative to NoCorr-CBCT (light gray bars in both plots; $p = 0.05$). Root-mean-square uncertainty in the reproducibility of localization discrepancy [5 measurements per case; error bars in Fig. 6(a)] is 0.2 mm. Figure 6(b) shows that differences in localization discrepancy between RMC-CBCT(sim) and RMC-CBCT(tx) are less than 2 mm in almost all cases (dark gray bars).

Figure 7(a) compares NCC inside the VOI enclosing the GTV for the three types of CBCT images with respect to the gated CBCT. Results are sorted in order of decreasing difference in NCC [RMC-CBCT(tx) minus NoCorr-CBCT].

Figure 7(b) shows differences in NCC between RMC-CBCT(tx) and NoCorr-CBCT, and between RMC-CBCT(tx) and RMC-CBCT(sim). In 21 out of 22 cases, NCC is higher in RMC-CBCT(tx) relative to NoCorr-CBCT ($p < 0.0001$; light gray bars in both plots). NCC in RMC-CBCT(tx) is larger in 12 out of 22 cases relative to RMC-CBCT(sim) and differences in most cases are small and not significant [$p = 0.84$; dark gray bars in Fig. 7(b)].

To evaluate the robustness of our motion correction technique, we studied the dependency of tumor localization discrepancy on tumor excursion and surrogate motion, measured as the difference in tumor centroid positions and diaphragm apex points between end-expiration and end-inspiration images in the RCCT from which motion correction is derived. Figure 8 compares the scatter plot of the difference in localization discrepancy [RMC-CBCT(sim) minus NoCorr-CBCT] vs tumor EE-to-EI excursion in RCCT(sim) based on (a) RCCT at simulation and (b) RCCT at treatment. Figure 8(b) shows that the improvement (Tx-NoCorr) is greater than 2 mm in three tumors, all of them belonging to the same patient. In this case, the improvement was large because the tumor motion in the RCCT on the treatment day was large (10.3, 12.6, 13.8 mm) and more than the motion at simulation (7.0, 8.6, 8.1 mm).

The data indicate that for tumor excursions less than 5 mm (dashed lines), motion correction yields only a modest reduction in localization discrepancy of 1 mm or less. This applies to motion correction based on both RCCT at simulation and treatment.

4. DISCUSSION AND CONCLUSIONS

In a prospective study of 19 lung cancer patients (22 tumors), we have evaluated the efficacy of RMC-CBCT to reduce motion artifacts and improve localization accuracy. The study examined end expiration as the motion-corrected state, which

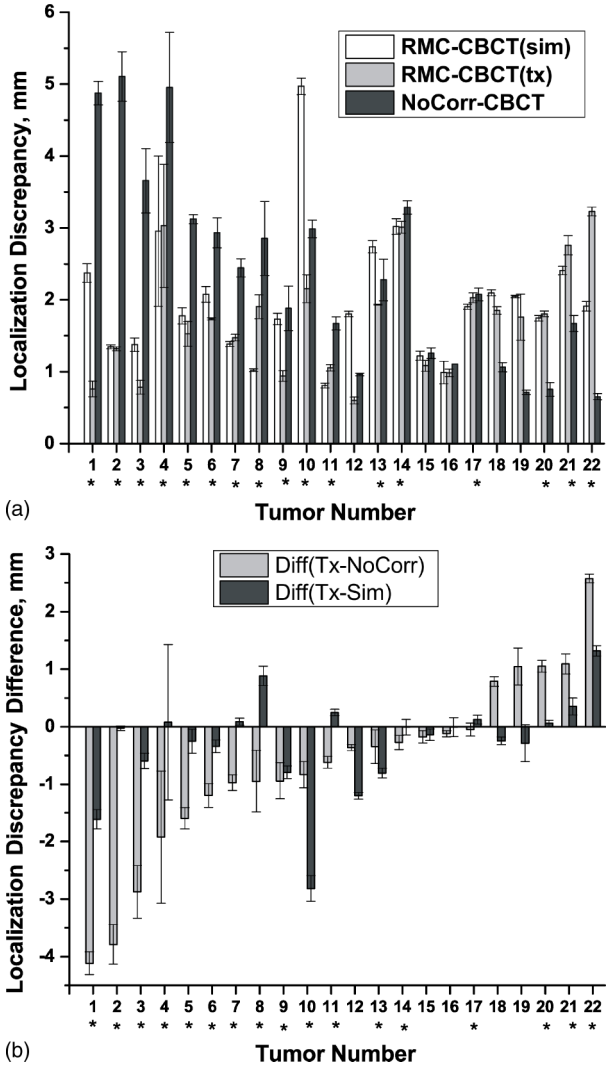

FIG. 6. (a) Tumor localization discrepancy before motion correction (NoCorr-CBCT), after motion correction derived from RCCT at treatment [RMC-CBCT(tx)], and after correction derived from RCCT at simulation [RMC-CBCT(sim)]. (b) Difference in localization discrepancy between RMC-CBCT(tx) and NoCorr CBCT, and between RMC-CBCT(tx) and RMC-CBCT(sim) CBCT. In both plots, tumor cases are sorted in order of increasing difference in localization discrepancy (RMC-CBCT(tx) minus NoCorr). Column bars indicate mean localization discrepancy from five measurements; error bars indicate standard deviation. Asterisks indicate cases in which tumor EE-to-EI excursion in the RCCT at treatment is 5 mm or more.

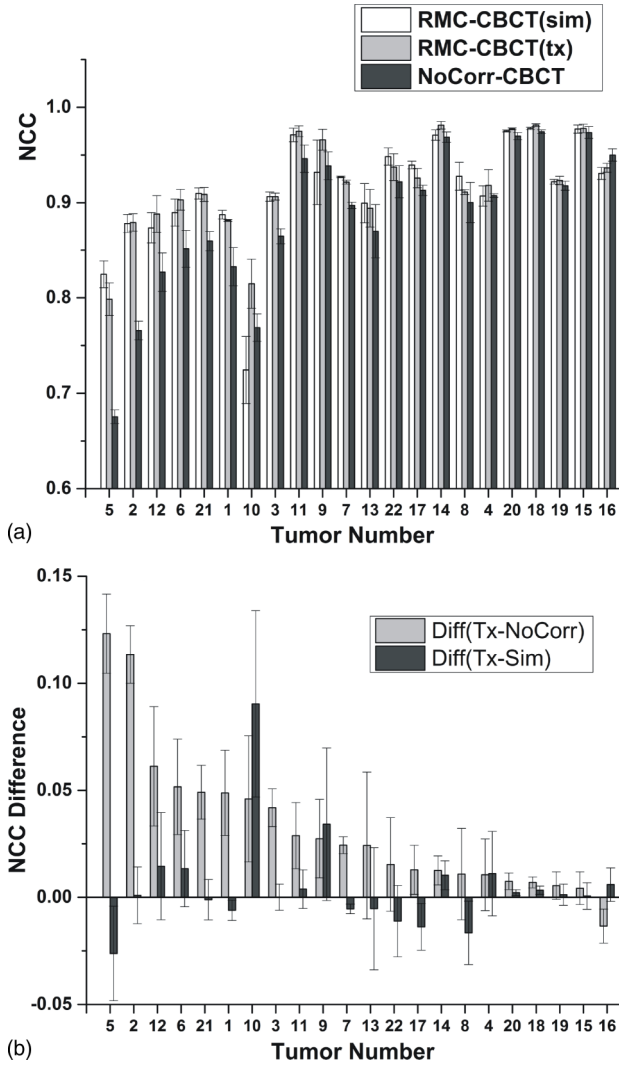

FIG. 7. (a) NCC inside a VOI around the tumor in CBCT images before and after motion correction, following rigid registration with the gated CBCT. (b) Difference in NCC between RMC-CBCT(tx) and NoCorr CBCT, and between RMC-CBCT(tx) and RMC-CBCT(sim) CBCT. In both plots, tumor cases are sorted in order of decreasing difference in NCC (RMC-CBCT(tx) minus NoCorr). Column bars indicate mean NCC from five measurements; error bars indicate standard deviation.

allowed comparison to a gated CBCT technique, also acquired at end expiration, as a criterion standard.

Our findings show that the motion-correction method reduces localization discrepancy (Fig. 6) and motion blurring (Figs. 5 and 7) in most cases. The observed correlation in RCCT between tumor motion and ipsilateral diaphragm motion (Fig. 4) supports the validity of choosing the latter as a surrogate for controlling the amount of motion correction.

A second study goal examined whether the motion correction derived from a RCCT at simulation yields similar tumor localization accuracy so it can be used for motion-corrected CBCT at treatment. Motion correction at end expiration using a RCCT acquired at simulation was found to yield similar results to those using a RCCT on the treatment day, 2–3 weeks after simulation [Fig. 6(b)]. These findings suggest that the RCCT at simulation may be sufficiently accurate for motion-corrected CBCT early on in treatment in most cases; however, the study did not examine whether this conclusion remains valid for CBCT scans acquired later in the treatment course.

A further study finding is that the achieved reduction in localization discrepancy with motion-corrected CBCT depends on the amount of tumor motion. This is evidenced by the larger fraction of cases showing reduced localization discrepancy when tumor motion is 5 mm or more (Fig. 6), and by the larger reductions in localization discrepancy in cases with larger tumor motion (Fig. 8). The data suggest that the tumor motion observed in the RCCT at simulation can be used as a predictor to determine which cases may benefit from motion-corrected CBCT [Fig. 8(a)]. These findings are in good agreement with other groups.[23]

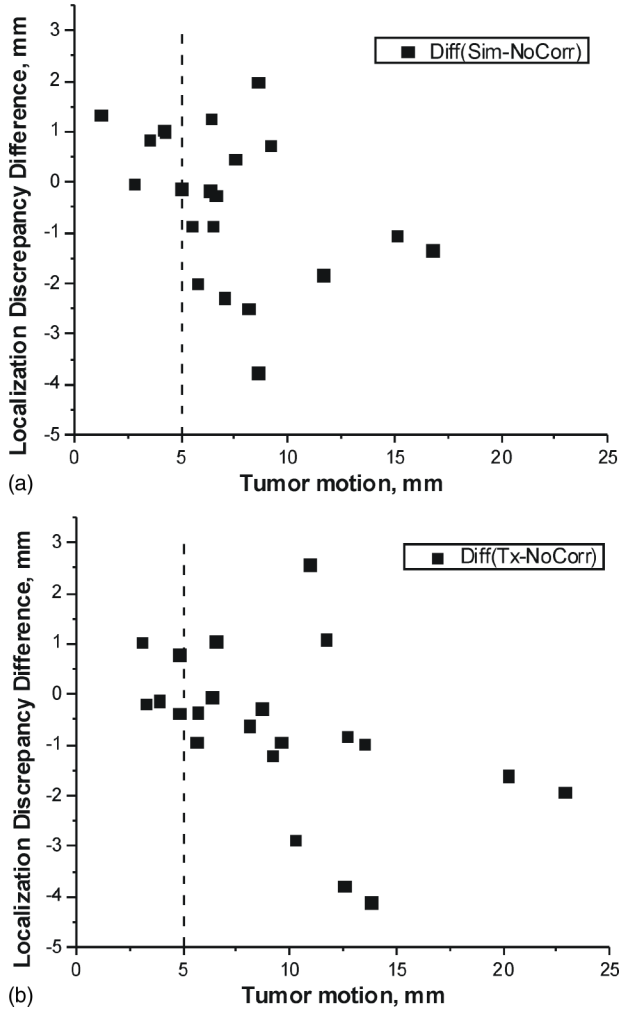

FIG. 8. Scatter plot of the difference in localization discrepancy [RMC-CBCT(sim) minus NoCorr-CBCT] vs tumor EE-to-EI excursion in RCCT based on (a) RCCT at simulation and (b) RCCT at treatment.

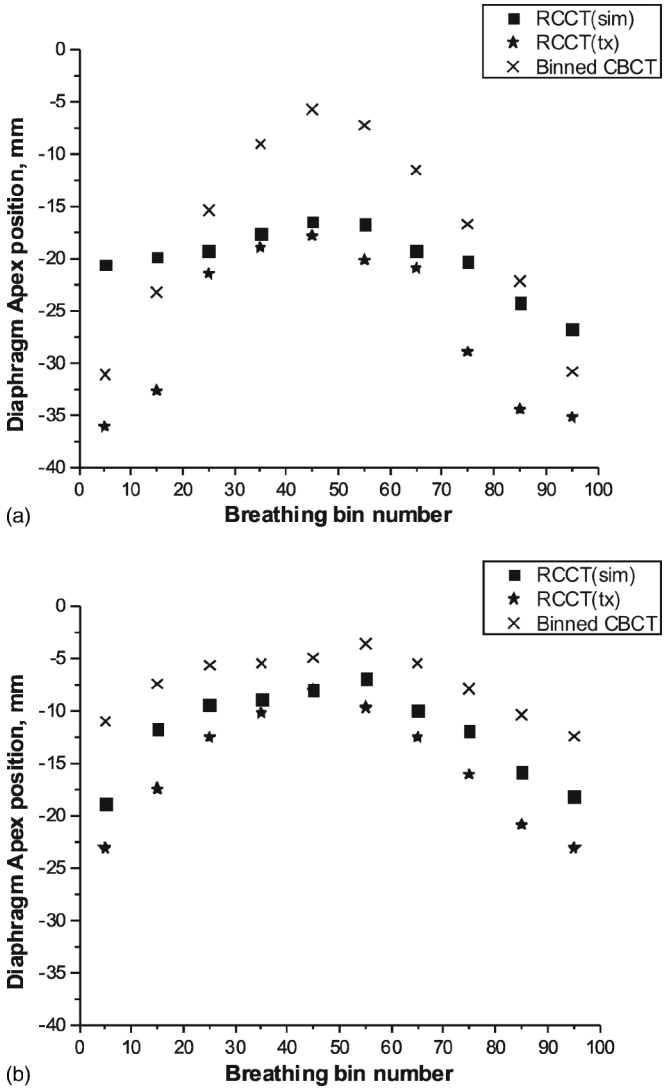

FIG. 9. Diaphragm apex position vs amplitude-sorted bin, from RCCT(sim), RCCT(tx), and binned CBCT image sets: (a) tumor number 10 and (b) tumor number 22. See text for details.

One limitation of the method occurs in cases where respiratory motion at treatment is larger than at simulation, thus requiring extrapolation of the motion model beyond the range of motions of the RCCT image set from which it is derived. Figure 9 shows the diaphragm apex motion patterns (i.e., position vs amplitude-sorted bin number) in the image sets of two patient cases.

In one patient case, the RCCT(sim) showed small diaphragm excursion [Fig. 9(a), squares], whereas diaphragm excursion in the CBCT was larger (crosses). Due to shallow breathing on the simulation day, the RCCT(sim) data set exhibited little motion, thus underestimating the amount of motion correction in the CBCT: This resulted in increased localization discrepancy [Fig. 6(a), tumor number 10, RMC-CBCT(sim)] and decreased NCC [Fig. 7(a), tumor number 10, RMC-CBCT(sim)].

Another limitation, mentioned above, occurs when there is little motion in the CBCT [Fig. 9(b), crosses]. In this case localization discrepancy without motion correction is already small and uncertainties in the motion correction procedure may result in increased localization discrepancy [Fig. 6(a), tumor number 22].

In our motion model, the ipsilateral diaphragm apex is used as a surrogate to control the amount of motion correction, i.e., to determine the 3D deformation to apply to each binned CBCT. The choice of ipsilateral diaphragm as surrogate assumes that there is less variation in the motion model between RCCT and CBCT for organs that are in closer proximity to the surrogate. Conversely, the motion model may less accurately predict deformations of contralateral organs in some cases. An example is illustrated in Fig. 10 in which the gated CBCT (in green) is overlaid with the RMC-CBCT(tx) (in red). It shows that concordance of anatomy between the two images is higher on the ipsilateral side (patient's left) indicating that constancy of the deformation-surrogate relationship is diminished on the contralateral side. We note that in this instance localization accuracy is not adversely affected, as can be seen in the region of the tumor (arrow).

Rit *et al.* reported in their study that CBCT images acquired within 1 min can provide good localization accuracy of the tumor and improved image quality if the respiratory

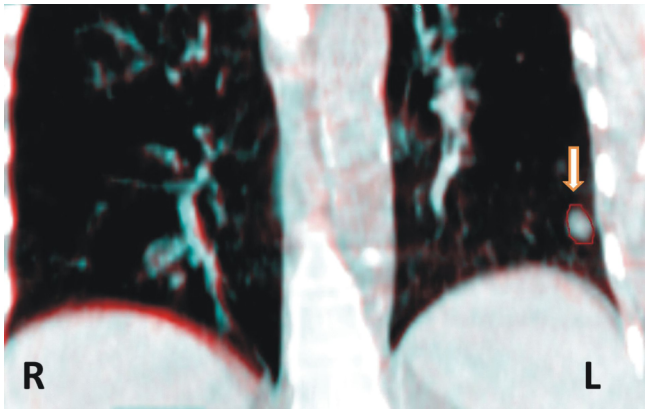

FIG. 10. Overlay of gated CBCT (green enhanced) and RMC-CBCT(tx) (red) images, for tumor number 22. Choice of diaphragm on the ipsilateral side (patient's left, labeled L) results in higher soft tissue concordance on that side. Arrow indicates location of GTV.

motion correction has been applied.[23] For validation of these results they used RCCT–CBCT as a standard for comparison. In such approach, however, image quality suffers from view aliasing artifacts which limits its utility as a criterion standard. In this study, we used gated CBCT which yields a high-quality CBCT which allows a more reliable measure of localization discrepancy.[11]

In its clinical application, motion-corrected CBCT allows reconstruction at respiration motion states that is relevant to treatment. In radiation treatments involving motion management, a consistent patient geometry and motion state is desirable for imaging and treatment.[24,25] In this study, RMC-CBCT reconstructions were carried out at end expiration. The observed improved agreement in lung tumor position between RMC-CBCT and (end-expiration) gated CBCT, relative to that between NoCorr-CBCT and gated CBCT, underscores the applicability of RMC-CBCT to gated treatment at end expiration. For determination of patient position correction, registration of the RMC-CBCT would be to the simulation RCCT image near end expiration. Although not examined in this study, motion-corrected CBCT may also be reconstructed at a respiration-averaged position, which is more suitable for treatment without active motion management. In this instance, a midposition RCCT reference image[26] would serve for construction of the motion model and correction.

ACKNOWLEDGMENTS

This work was supported in part by Award Number R01-CA126993 from the National Cancer Institute and a research agreement with Varian Medical Systems. The content is solely the responsibility of the authors and does not necessarily represent the official views of the National Cancer Institute or the National Institutes of Health. We thank Timo Berkus for assistance with the Varian iTools CBCT reconstruction software.

[a]Author to whom correspondence should be addressed. Electronic mail: magerasg@mskcc.org; Telephone: 646-888-5615.

[1]S. S. C. Burnett, K. E. Sixel, P. C. F. Cheung, and J. D. P. Hoisak, "A study of tumor motion management in the conformal radiotherapy of lung cancer," Radiother. Oncol. **86**(1), 77–85 (2008).

[2]P. J. Keall, G. S Mageras, J. M. Balter, R. S. Emery, K. M. Forster, S. B. Jiang, J. M. Kapatoes, D. A. Low, M. J. Murphy, B. R. Murray, C. R. Ramsey, M. B. Van Herk, S. S. Vedam, J. W. Wong, and E. Yorke, "The management of respiratory motion in radiation oncology report of AAPM Task Group 76," Med. Phys. **33**(10), 3874–3900 (2006).

[3]N. Clements, T. Kron, R. Franich, L. Dunn, P. Roxby, Y. Aarons, B. Chesson, S. Siva, D. Duplan, and D. Ball, "The effect of irregular breathing patterns on internal target volumes in four-dimensional CT and cone-beam CT images in the context of stereotactic lung radiotherapy," Med. Phys. **40**(2), 021904 (10pp.) (2013).

[4]J.-J. Sonke, L. Zijp, P. Remeijer, and M. van Herk, "Respiratory correlated cone beam CT," Med. Phys. **32**(4), 1176–1186 (2005).

[5]T. Li, L. Xing, P. Munro, C. McGuinness, M. Chao, Y. Yang, B. Loo, and A. Koong, "Four-dimensional cone-beam computed tomography using an on-board imager," Med. Phys. **33**(10), 3825–3833 (2006).

[6]J. Lu, T. M. Guerrero, P. Munro, A. Jeung, P. C. Chi, P. Balter, X. R. Zhu, R. Mohan, and T. Pan, "Four-dimensional cone beam CT with adaptive gantry rotation and adaptive data sampling," Med. Phys. **34**(9), 3520–3529 (2007).

[7]J.-P. Bissonnette, K. N. Franks, T. G. Purdie, D. J. Moseley, J.-J. Sonke, D. A. Jaffray, L. A. Dawson, and A. Bezjak, "Quantifying interfraction and intrafraction tumor motion in lung stereotactic body radiotherapy using respiration-correlated cone beam computed tomography," Int. J. Radiat. Oncol., Biol., Phys. **75**(3), 688–695 (2009).

[8]J.-P. Bissonnette, T. G. Purdie, J. A. Higgins, W. Li, and A. Bezjak, "Cone-beam computed tomographic image guidance for lung cancer radiation therapy," Int. J. Radiat. Oncol., Biol., Phys. **73**(3), 927–934 (2009).

[9]T. G. Purdie, J.-P. Bissonnette, K. Franks, A. Bezjak, D. Payne, F. Sie, M. B. Sharpe, and D. A. Jaffray, "Cone-beam computed tomography for on-line image guidance of lung stereotactic radiotherapy: Localization, verification, and intrafraction tumor position," Int. J. Radiat. Oncol., Biol., Phys. **68**(1), 243–252 (2007).

[10]T. G. Purdie, D. J. Moseley, J.-P. Bissonnette, M. B. Sharpe, K. Franks, A. Bezjak, and D. A. Jaffray, "Respiration correlated cone-beam computed tomography and 4DCT for evaluating target motion in stereotactic lung radiation therapy," Acta Oncol. **45**(7), 915–922 (2006).

[11]R. E. Kincaid, E. D. Yorke, K. A. Goodman, A. Rimner, A. J. Wu, and G. S. Mageras, "Investigation of gated cone-beam CT to reduce respiratory motion blurring," Med. Phys. **40**(4), 041717 (11pp.) (2013).

[12]J. P. Santoro, J. McNamara, E. Yorke, H. Pham, A. Rimner, K. E. Rosenzweig, and G. S. Mageras, "A study of respiration-correlated cone-beam CT scans to correct target positioning errors in radiotherapy of thoracic cancer," Med. Phys. **39**(10), 5825–5834 (2012).

[13]J.-J. Sonke, J. Lebesque, and M. van Herk, "Variability of four-dimensional computed tomography patient models," Int. J. Radiat. Oncol., Biol., Phys. **70**(2), 590–598 (2008).

[14]J. C. Park, S. H. Park, J. H. Kim, S. M. Yoon, S. Y. Song, Z. Liu, B. Song, K. Kauweloa, M. J. Webster, A. Sandhu, L. K. Mell, S. B. Jiang, A. J. Mundt, and W. Y. Song, "Liver motion during cone beam computed tomography guided stereotactic body radiation therapy," Med. Phys. **39**(10), 6431–6442 (2012).

[15]M. Brehm, P. Paysan, M. Oelhafen, P. Kunz, and M. Kachelriess, "Self-adapting cyclic registration for motion-compensated cone-beam CT in image-guided radiation therapy," Med. Phys. **39**(12), 7603–7618 (2012).

[16]T. Li and L. Xing, "Optimizing 4D cone-beam CT acquisition protocol for external beam radiotherapy," Int. J. Radiat. Oncol., Biol., Phys. **67**(4), 1211–1219 (2007).

[17]P. T. Lauzier, J. Tang, and G.-H. Chen, "Prior image constrained compressed sensing: Implementation and performance evaluation," Med. Phys. **39**(1), 66–80 (2011).

[18]S. Rit, J. W. H. Wolthaus, M. van Herk, and J.-J. Sonke, "On-the-fly motion-compensated cone-beam CT using an a priori model of the respiratory motion," Med. Phys. **36**(6), 2283–2296 (2009).

[19]Q. Zhang, Y.-C. Hu, F. Liu, K. Goodman, K. E. Rosenzweig, and G. S. Mageras, "Correction of motion artifacts in cone-beam CT using a patient-specific respiratory motion model," Med. Phys. **37**(6), 2901–2909 (2010).

[20]A. Hertanto, Q. Zhang, Y.-C. Hu, O. Dzyubak, A. Rimner, and G. S. Mageras, "Reduction of irregular breathing artifacts in respiration-correlated CT images using a respiratory motion model," Med. Phys. **39**(6), 3070–3079 (2012).

[21]R. George, P. J. Keall, V. R. Kini, S. S. Vedam, V. Ramakrishnan, and R. Mohan, "Is the diaphragm motion probability density function normally distributed," Med. Phys. **32**(2), 396–404 (2005).

[22]L. A. Feldkamp, L. C. Davis, and J. W. Kress, "Practical cone-beam algorithm," J. Opt. Soc. Am. A **1**(6), 612–619 (1984).
[23]S. Rit, J. Nijkamp, M. van Herk, and J.-J. Sonke, "Comparative study of respiratory motion correction techniques in cone-beam computed tomography," Radiother. Oncol. **100**(3), 356–359 (2011).
[24]S. B. Jiang, "Technical aspects of image-guided respiration-gated radiation therapy," Med. Dosim. **31**(2), 141–151 (2006).
[25]S. B. Jiang, J. Wolfgang, and G. S. Mageras, "Quality assurance challenges for motion-adaptive radiation therapy: Gating, breath holding, and four-dimensional computed tomography," Int. J. Radiat. Oncol., Biol., Phys. **71**(Suppl. 1), S103–S107 (2008).
[26]J. W. Wolthaus, J.-J. Sonke, M. van Herk, J. S. Belderbos, M. M. Rossi, J. V. Lebesque, and E. M. Damen, "Comparison of different strategies to use four-dimensional computed tomography in treatment planning for lung cancer patients," Int. J. Radiat. Oncol., Biol., Phys. **70**(4), 1229–1238 (2008).
[27]W. Lu, M. L. Chen, G. H. Olivera, K. J. Ruchala, and T. R. Mackie, "Fast free-form deformable registration via calculus of variations," Phys. Med. Biol. **49**, 3067–3087 (2004).